IEEE Access
Multidisciplinary | Rapid Review | Open Access Journal

Received 29 March 2023, accepted 17 April 2023, date of publication 21 April 2023, date of current version 26 April 2023.

Digital Object Identifier 10.1109/ACCESS.2023.3269288

RESEARCH ARTICLE

A Sensor-Based Modified FMD Method to Identify Fault Feature for Mechanical Fault Diagnosis of Ship-Borne Antennae

ZIPENG LI[1,2], ZITONG ZHOU[3], AND XIAOYI ZHOU[1,2]

[1]School of Marine Science and Technology, Northwestern Polytechnical University, Xi'an 710072, China
[2]Key Laboratory of Ocean Acoustics and Sensing, Ministry of Industry and Information Technology, Northwestern Polytechnical University, Xi'an 710072, China
[3]Shaanxi Key Laboratory of Gear Transmission, Shaanxi Fast Company Ltd., Xi'an 710117, China

Corresponding author: Zipeng Li (class1lizp@163.com)

This work was supported by the China Postdoctoral Science Foundation under Grant 2021M692628, in part by the National Natural Science Foundation of China under Grant 42076198, and in part by the Science and Technology on Sonar Laboratory Foundation under Grant 6142109KF212205.

ABSTRACT It is necessary to perform condition monitoring and fault identification on ship-borne antennae to ensure navigation safety. However, timely fault identification of key parts in a complicated drivetrain of the ship-borne antenna is still a challenging task since fault features are usually modulated and inevitably submerged by heavy noise. Therefore, a new adaptive feature extraction method based on Feature Mode Decomposition (FMD) is proposed in this paper for diagnostic purpose. First, scale transform is applied on the spectrum of the monitoring signal to determine the parameters of FMD, including the number of FIR filters, the location of each filter and the order of the filter bank. Second, a modified feature mode decomposition (MFMD) algorithm is proposed to adaptively extract mono-component modes and combine similar modes for weak feature enhancement. Finally, the combined modes are analyzed for mechanical fault identification based on Hilbert demodulation. Two application cases show that the proposed method owns superior performance during feature extraction, compared with the traditional methods.

INDEX TERMS Mechanical fault diagnosis, feature extraction, feature mode decomposition, ship-borne antenna transmission system.

I. INTRODUCTION

Due to severe marine environment, complex load and long-term operation, key mechanical parts of ship-borne antennae inevitably degenerate and malfunction in different forms. Mechanical faults of key components may cause various serious accidents, causing operation accident eventually. Therefore, fault location and identification are of reasonable significance for navigation safety [1], [2], [3].

Feature extraction, which extract the hidden fault-related information from the raw monitoring signal, is one of the most important steps in the antenna fault diagnosis [4], [5], [6]. When a fault exists in one rotating machine, the vibration signal is mixed with periodic repetitive sharp peaks and further modulated by inherent multiples. The aim of feature extraction is to refine the periodic impulses from the complicated signal by filtering, demodulating and matching [7], [8]. However, conventional methods, such as deconvolution, Spectrum Kurtosis (SK) and Wavelet Packet (WT), are confronting incremental challenges, because complex structure and composition of ship-borne antennae seriously decrease the signal-to-noise ratio (SNR) of condition monitoring signals [9], [10], [11].

Recent years have witnessed a rapid development of signal decomposition methods. Decomposition methods can divide the original signal into simple parts, and each single part is far more easily analysed than the original signal [12]. Among them, Empirical Mode Decomposition (EMD), proposed by Huang, is the most classic and famous adaptive decomposition method. It can divide the signal into several

The associate editor coordinating the review of this manuscript and approving it for publication was Yiqi Liu.

orthogonal modes, which are so-called "Intrinsic Mode Function (IMF)", by utilizing the local time-scales decomposition criterion [13]. Since EMD appears, it has shown huge potential in the mechanical fault diagnosis and has achieved great success [14], [15], [16], [17], [18]. However, the result of EMD highly depends on the extremum seeking algorithm and the ending criterion. Inevitable end effects and the mode mixing problem will restrict the application of EMD [19].

To enhance the performance of EMD and solve the mode mixing problem, substantial numbers of improved methods, such as Ensemble Empirical Mode Decomposition (EEMD) and Local Mean Decomposition (LMD), are proposed. EEMD, a modified EMD method, reduces the influence of background noise by harmonic test and population average [20]. In 2018, Mohammad et al. achieved quantitative bearing fault diagnosis by using improved ensemble empirical mode decomposition [21]. In 2019, Li et al. combined EEMD and frequency band entropy for bearing fault feature extraction and validated the effectiveness of the proposed method through an experimental data set [22]. In 2021, Li et al. proposed an improved EEMD based on the improved adaptive resonance technology (IART), and it can select the optimal IMF(s) according to the resonance frequency of IART [23].

As for LMD, it is an adaptive decomposition method based on the local extremum moving average theory [24]. In 2018, Zhao et al. proposed a compound interpolation envelope LMD method for fault diagnosis of reciprocating compressors and validated the effectiveness of the proposed approach through practical vibration signals [25]. In 2021, Sharma combined multi-scale-fluctuation-based dispersion entropy and LMD to analysis the bearing faults, and the result shows that the proposed method has potential for gaining further insights into the dynamics of rotary machines [26]. Although a series of effective improvements have been implemented to solve problems caused by incomplete decomposition theories, EMD, EEMD and LMD are essentially recursive, and never consider the form of fault feature.

Encouragingly, two non-recursive methods, empirical wavelet transform (EWT) and variational mode decomposition (VMD) were proposed and introduced into the mechanical fault diagnosis. EWT is a non-recursive decomposition method, which decomposes the signal into adaptive subband signals and constructs corresponding basis functions for wavelet transform. Pan proposed an improved data-driven EWT method and used the proposed approach to extract weak bearing fault features [27]. Saeed used EWT to denoise vibration monitoring signals and the comparison shows a better result than the EMD-denoising technique [28]. Although EWT evades the accumulative error problem, the binary band segmentation strategy may mislead EWT to divide the characteristic signal into different modes.

VMD, which is proposed by Konstantin and Dominique, can design a group of Wiener filters, and then divide the raw signal into several modes with different centre frequencies through the Wiener filter bank [29]. Wang firstly discussed the relative merits of VMD and applied it to identify the rub-impact fault of the rotating machinery [30]. Furthermore, he found a perfect VMD result depends on appropriate choices of VMD parameters, including the number of modes, the balance parameter and the initial centre frequencies (ICFs). Therefore, various criteria, such as correlation coefficient [31] and Teager energy operator [32], are used to select optimal parameters. Meanwhile, intelligence optimization algorithms are also introduced and researched, such as genetic algorithm [33] and grasshopper optimization algorithm [34]. Typically, Miao chose grasshopper optimization algorithm to search the optimal parameters for VMD and verify its effectiveness through practical cases [35]. Although lots of parameter selection methods are proposed, it is still a hard challenge to use VMD without any prior knowledge.

Inspire by these mode decomposition methods, a novel adaptive decomposition algorithm, called Feature Mode Decomposition (FMD), is proposed by Miao recently [36]. FMD uses an adaptive FIR filter bank to decompose the raw signal into different modes, and a new criterion, correlated Kurtosis (CK), is built as the objective function to update the filter bank iteratively. However, the performance of FMD highly depends on the initial number of FIR filters [37]. Ref [37] solve this problem by designing a new index to optimize the parameters of FMD. But FMD also eliminates some meaningful modes during iteration, which is ignored in Ref [37].

In this paper, a modified FMD method aiming at ship-borne antenna drive-train fault identification is proposed. As an effective method to extract partition information in frequency spectrum, scale-space representation is used to determine the number of FIR filters and the location of them, as well as the order of the filter bank. With optimal parameters, the raw signal is decomposed into a series of mono-component modes potentially containing fault characteristics. Then empirical modes can be obtained by adaptively combining mono-components based on their similarity. Finally, the empirical mode with the largest correlated Kurtosis (CK) value is selected for demodulation analysis.

The rest of this paper is organized as follows: Section II discusses the structure of the diagnosis system for the ship-borne antenna; Section III and IV introduce the modified method and the simulation respectively; Two cases are introduced in Section V to prove the effectiveness of the proposed method; Finally, the conclusion is drawn in Section VI.

II. HEALTH MANAGEMENT SYSTEM FOR SHIP-BORNE ANTENNAE

A typical ship-borne satellite communication antenna is shown in Fig. 1. Usually, a ship-borne communication antenna contains three drive subsystems, which control crossing moving, pitching moving and rotating moving respectively. Furthermore, one drive subsystem usually consists of two identical transmission chains for anti-backlash, and each

transmission chain contains three key components: motor, planetary reducer, and transmission gear box. For condition monitoring and fault diagnosis, some accelerometer sensors are attached on the drive subsystems. For example, key components of the azimuth drivetrain with attached accelerometer sensors are shown in Fig. 2.

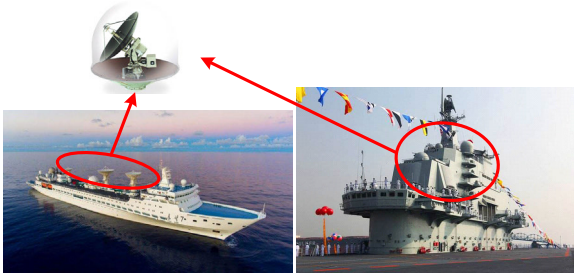

FIGURE 1. The ship-borne communication antenna on the ocean vessel.

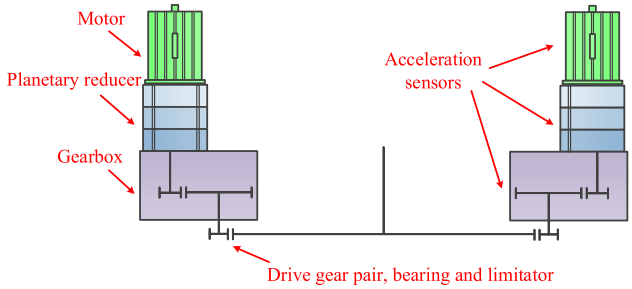

FIGURE 2. Key components of the azimuth drive-train with attached accelerometer sensors.

A health management system is also developed for condition monitoring and fault warning of the ship-borne antenna drive-train. The system is composed of accelerometer sensors, a data acquisition device, a signal processor, and diagnosis software, as Fig. 3 shows. When the system is working, vibration signals are collected and recorded first. Then, collected vibration signals are uploaded to the upper computer and the embedded diagnosis software extracts possible fault characteristics form the vibration signals. Finally, the health management system sounds the alarm according to the fault characteristics and fault degree.

The embedded health management software, which is designed based on LabVIEW, Matlab, and SQL Server, is the core of the system. It can work in two modes: condition monitoring mode and advanced diagnosis mode. The monitoring mode contains basic signal processing methods such as time domain analysis and statistical analysis, which are reliable to observe the longstanding behavioural trend of drivetrains. The diagnosis mode is used to identify mechanical faults based on signal decomposition methods such as wavelet transform, EMD and so on. The flowchart of the diagnosis procedure is shown in Fig. 4. Because of multi-modulation and heavy noise, more effective signal processing methods should be developed to improve the capacity of fault detection.

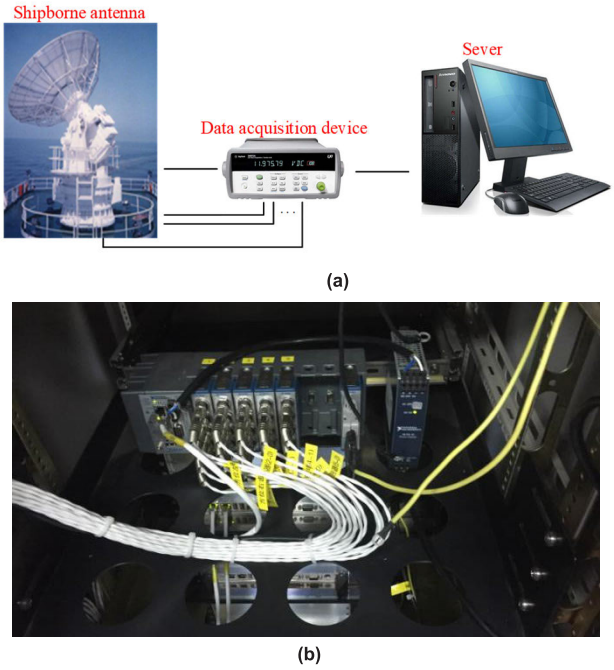

FIGURE 3. (a) The framework of the data acquisition device. (b) the data acquisition device.

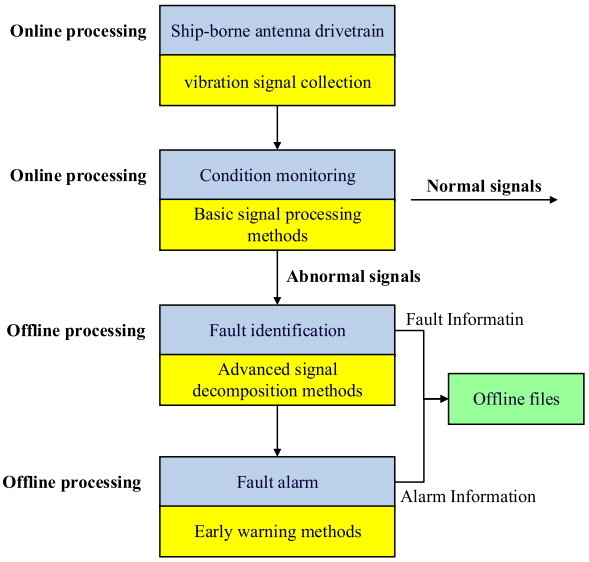

FIGURE 4. The flowchart of the diagnosis procedure.

III. THE PROPOSED METHOD

A. FEATURE MODE DECOMPOSITION THEORY

Inspired by VMD, FMD is also a non-recursive decomposition method, and designed to divide the raw signal into different modes adaptively by designing an FIR filter bank. Since the decomposition result highly depends on filter coefficients, FMD iteratively updates filter coefficients to make the filtered signal infinitely approach the deconvolution objective function. Therefore, the mode decomposition algorithm of FMD is finally regard as a solution of a constrained problem and

can be presented as:

$$\arg\max_{\{f_k(l)\}} \left\{ CK_M(u_k) = \frac{\sum_{n=1}^{N} \left(\prod_{m=0}^{M} u_k(n - mT_s) \right)^2}{\left(\sum_{n=1}^{N} u_k(n)^2 \right)^{M+1}} \right\}$$
$$s.t. u_k(n) = \sum_{l=1}^{L} f_k(l)\, x(n - l + 1) \quad (1)$$

Correlated Kurtosis (CK), which can evaluate the impulsiveness and periodicity of the signal, is chosen to be the objective function [38]. $u_k(n)$ is the kth decomposed mode, $f_k(l)$ is the kth FIR filter with length L, T_s is the input period and M denotes the order of shift.

Eq. (1) can be solved with an iterative eigenvalue decomposition algorithm. First, we rewrite the decomposition mode as a matrix form:

$$u_k = \begin{bmatrix} u_k(1) \\ \cdots \\ u_k(N - L + 1) \end{bmatrix} = Xf_k = \begin{bmatrix} x(1) & \cdots & x(L) \\ \vdots & \ddots & \vdots \\ x(N - L + 1) & \cdots & x(N) \end{bmatrix} \begin{bmatrix} f_k(1) \\ \cdots \\ f_k(L) \end{bmatrix} \quad (2)$$

Then, the CK of each mode can be defined as:

$$CK_M(u_k) = \frac{u_k^H W_M u_k}{u_k^H u_k} \quad (3)$$

where H is the conjugate transpose operation, W_M is an intermediate variable for the weighted correlation matrix and as in (4), shown at the bottom of the page.

Combining (2) and (3), we gain the final expression of the objective function:

$$CK_M(u_k) = \frac{f_k^H X^H W_M X f_k}{f_k^H X^H X f_k} = \frac{f_k^H R_{XWX} f_k}{f_k^H R_{XX} f_k} \quad (5)$$

where R_{XWX} and R_{XX} are the weighted correlation matrix and the correlation matrix, respectively. Until now, we gain the updating method of the kth filter coefficients according to the solution of (5), and mono-component modes can be obtained by using the optimized FIR filter bank.

However, these mono-component modes might contain the same fault feature because of multi-modulation and some modes are meaningless noise components. To eliminate the redundant modes and reduce computation, FMD designs an iterative algorithm. After each decomposition, two modes with the biggest similarity are firstly selected and subsequently the one with less CK is abandoned from the two modes. Therefore, the new input signal is reconstructed by the remaining modes.

The flowchart of FMD algorithm is shown in Fig 5.

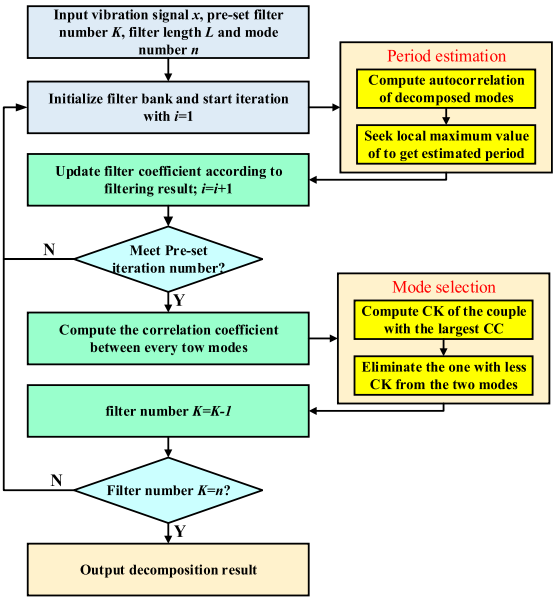

FIGURE 5. The flow chart of FMD algorithm.

B. MFMD

It is obvious that there are still two problems existing: First, the number of filters and the order of the filter bank highly influence the performance of the decomposition, but they are casually determined in the original FMD method. Second, FMD selected a complex and iterative mode selection algorithm, which not only eliminates some meaningful modes containing fault information, but also brings huge computational burden. Aiming at two problems above, we introduce an adaptive parameter selection method based on scale space expression and a non-recursive mode selection method based on the principle of similarity, proposing a modified FMD method. Unlike the original FMD algorithm, the decomposition is implemented only once in MFMD, which reduces a great deal of computation time.

1) SCALE SPACE EXPRESSION

Considering a discrete time signal $s(t)$, its frequency spectrum $S(f)$ is also discrete and can be defined as:

$$S(f) = \sum_{-\infty}^{+\infty} s(t)\, e^{-2j\pi ft} \quad (6)$$

$$W_M = \begin{bmatrix} \left(\prod_{m=0}^{M} u_k[1 - mT_s] \right)^2 & 0 & \cdots & 0 \\ 0 & \left(\prod_{m=0}^{M} u_k[2 - mT_s] \right)^2 & \cdots & 0 \\ \vdots & \vdots & \ddots & \vdots \\ 0 & 0 & \cdots & \left(\prod_{m=0}^{M} u_k[N - L + 1 - mT_s] \right)^2 \end{bmatrix} \frac{1}{\sum_{n=1}^{N-L+1} u_k[n]^{M-1}} \quad (4)$$

The scale space expression of a certain discrete signal in frequency domain can be defined as a convolution between its frequency spectrum and a kernel function [39]:

$$X(f,\delta) = g(f,\delta) * S(f) = \sum_{-\infty}^{+\infty} g(\tau,\delta) S(f-\tau) \quad (7)$$

As (7) shows, $X(f,\delta)$ can be explained as a non-local trend of the signal under a certain scale parameter δ. It removes detailed local characteristics and represents a macroscopic observation result of the frequency spectrum.

The Gaussian kernel function is selected as the optimal kernel function, because it has a similar shape to mono-component of the raw signal in the frequency domain:

$$g(f,\delta) = \frac{1}{\sqrt{2\pi\delta}} e^{-\frac{f^2}{2\delta}} \quad (8)$$

where δ is the scale factor. Substituting (8) in (7), the scale space expression of a discrete time signal can be obtained:

$$X(f,\delta) = g(f,\delta) * S(f) = \sum_{-M}^{+M} \frac{1}{\sqrt{2\pi\delta}} e^{-\frac{\tau^2}{2\delta}} \cdot S(f-\tau) \quad (9)$$

Since a truncated narrow neighbourhood can just satisfy the accuracy of the convolution, M is set to be $6\sqrt{\delta}+1$ in (9). Therefore, once a particular scale parameter δ is determined, we can naturally obtain a specific scale space expression of the raw vibration signal.

Unlike calculating all the scale space curves in different scale parameters, we can calculate only one scale domain curve with an optimal scale parameter δ when partitioning mono-components for fault diagnosis. Considering that each decomposed mono-component should contain fault information, the scale parameter should be larger than the fault characteristic frequency, which means $\sqrt{\delta} \geq \lambda f_r$ (f_r is the rotating frequency). Furthermore, mechanical fault characteristics, such as bearing faults, are usually $3f_r \sim 6f_r$, so the scale parameter is set to be $\sqrt{\delta} = 6f_r$ in this paper.

2) FMD PARAMETER DETERMINATION

Once the scale parameter δ is set and the scale space expression $X(f,\delta)$ is obtained, each local maximum in $X(f,\delta)$ is regarded as a symbol of a FIR filter and each filter can be partitioned by adjacent local minima. In other words, the number of filters can be determined as the number of local maxima. The upper and lower passing frequencies of each filter are assigned by the frequencies of adjacent local minima, while the upper and lower cut-off frequencies of each filter are determined according to the adjacent local maxima.

The order of the filter bank can be determined as follow: when designing a FIR filter using the window function method, we determine the order of the filter N as (10) shows:

$$\Delta f = \frac{d\omega}{N} \quad (10)$$

where $\Delta f = \min\left[\left|f_{pl} - f_{cl}\right|, \left|f_{pu} - f_{cu}\right|\right]$ is the actual width of the transition band, and $\frac{d\omega}{N}$ is decided by the type of the window function. Since the Hanning window is chosen in FMD, we have (11):

$$\min\left[\left|f_{pl} - f_{cl}\right|, \left|f_{pu} - f_{cu}\right|\right] = \frac{6.6\pi}{N} \quad (11)$$

Meanwhile, because we use a fixed order N to design the filter bank, this order N has to satisfy all filters in the bank. Therefore, N is computed by eq. (12):

$$N = \frac{6.6\pi}{\min\left[\left|f_{pl}^k - f_{cl}^k\right|, \left|f_{pu}^k - f_{cu}^k\right|\right]} \quad (12)$$

where k means the kth band. Eq (12) means that we choose the shortest transition band to compute the order N of the filter bank in fact.

3) MODE MERGING AND SELECTING

By using scale space expression, we detect spectrum boundaries and then decompose the signal into a set of modes via FMD with an optimal FIR filter bank. Each mode may potentially carry fault feature, and even some of them carries similar fault-related information because of multi-modulation. Therefore, mode merging and selecting based on similarity is necessary.

First, the similarity between any two modes can be defined according to Pearson's correlation coefficient (CC):

$$\gamma_{i,j} = \left| \frac{\sum_{t=o}^{T} \left(f_i(t) - a_i\right)\left(f_j(t) - a_j\right)}{\sqrt{\sum_{t=o}^{T} \left(f_i(t) - a_i\right)^2} \sqrt{\sum_{t=o}^{T} \left(f_j(t) - a_j\right)^2}} \right| \quad (13)$$

where $a_i = \frac{1}{T}\sum_{t=0}^{T} f_i(t)$ and $a_j = \frac{1}{T}\sum_{t=0}^{T} f_j(t)$. Second, we set the threshold value of CC to be 0.2 in this paper. In other words, if the value of CC between two mono-component modes is larger than 0.2, they are considered to be similar and should be combined. After combining, we obtain several empirical modes and then select the empirical mode which satisfies following conditions for fault feature extraction:

1. It must contain the mode with the largest CK;
2. Among all empirical modes which contains the mode with the largest CK, it must consist of the most raw modes.

4) PROCEDURE OF MFMD

Until now, the procedure of MFMD can be summarized and the flow chart is shown in Fig. 6:

(1). Obtain the Fourier spectrum of the raw signal.

(2). Compute the scale space expression of the Fourier spectrum and determine the parameters of FMD.

(3). Decompose the raw signal into a series of mono-component modes.

(4). Calculate the envelope spectrum of each mode and compute the correlation coefficients between any two modes.

(5). Combine modes according to the corresponding correlation coefficients.

(6). Select the empirical mode based on CK and extract fault features.

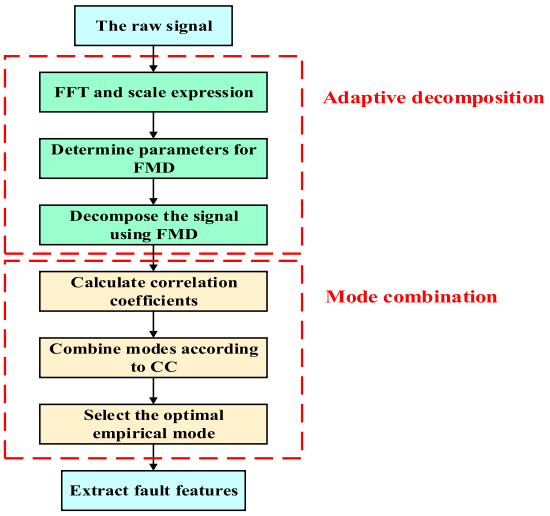

FIGURE 6. The flow chart of MFMD.

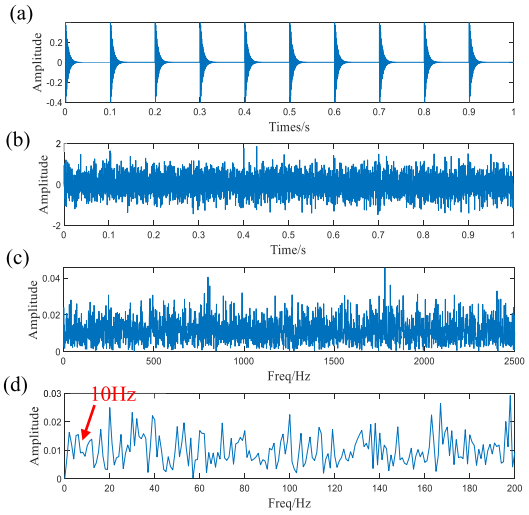

FIGURE 7. (a) The impulse response. (b) the noisy signal. (c) the spectrum of the noisy signal. (d) the envelope spectrum of the noisy signal.

IV. SIMULATION EXPERIMENT

For clear discussion of the proposed method, a periodical impulse response simulation signal is formulated first. White Gaussian noise with the signal-to-noise ratio (SNR) per sample in -10 dB is also added to the simulated signal, and the noisy testing signal is expressed as:

$$x(t) = \sum_i A e^{-2\pi f_i \beta (t-t_i)} \cos\left(2\pi f_i (t - t_i)\right) + n(t) \quad (14)$$

where $t_i = \frac{i}{f_r}$, A stands for the amplitude, and $\beta = 0.035$ denotes the damping characteristic of the system. The occurrence rate of the repetitive impulses f_r is set to be 10 Hz. The sampling rate of the testing signal is 5000 Hz and the sampling interval is 1s. The impulse response is displayed in Fig. 7(a), while the noisy signal is shown in Fig. 7(b). The frequency spectrum and the envelope spectrum of the noisy signal are displayed in Fig. 7(c) and Fig. 7(d) respectively, in which the characteristic frequency 10 Hz is buried.

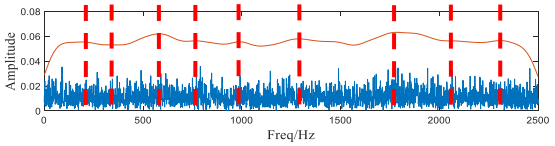

FIGURE 8. The scale expression of the frequency spectrum.

TABLE 1. Correlation coefficients.

	Mode 1	Mode 2	Mode 3	Mode 4	Mode 5	Mode 6	Mode 7	Mode 8	Mode 9
Mode 1	1	0.032	-0.106	-0.050	0.063	-0.015	-0.039	-0.052	0.040
Mode 2	-	1	0.025	0.038	0.031	0.059	0.014	0.048	0.023
Mode 3	-	-	1	0.118	-0.015	-0.006	0.437	0.363	0.040
Mode 4	-	-	-	1	0.092	-0.013	0.043	0.073	-0.024
Mode 5	-	-	-	-	1	-0.034	-0.009	-0.013	-0.005
Mode 6	-	-	-	-	-	1	0.058	0.085	0.061
Mode 7	-	-	-	-	-	-	1	0.562	0.047
Mode 8	-	-	-	-	-	-	-	1	0.033
Mode 9	-	-	-	-	-	-	-	-	1

Subsequently, MFMD is applied to this simulated signal. First, the frequency spectrum is represented in the scale domain as Fig. 8 shows. In Fig. 8, the blue line represents the Fourier spectrum of the raw signal; The orange line is the scale space expression of the Fourier spectrum; The red dotted lines represent the location of the local maximum points in the orange line. Therefore, the number of filters is set to be 9 according to the number of red dotted lines.

Meanwhile, the band with the narrowest transition band in Fig. 8 is the second band, so we select it to determine the order of the filter bank, and the result is 80. Then, the signal is decomposed into 9 modes based on the determined parameters, and the full results are shown in Fig. 9. The correlation coefficients between any two modes are calculated and shown in Table 1. According to table 1, mode 3, mode 7 and mode 8 are merged.

Figure 10 shows the envelop spectrum of mode 3, 7 and 8, while Fig. 11 shows the envelope spectrum of the combined mode. Compared with the original modes, the characteristic frequency and multiples in the combined mode are extraordinarily distinct, which proves the availability of MFMD.

As a comparison, the same signal is also analyzed by the original FMD method and VMD. First, the simulation signal is decomposed by FMD. The number of filters is set to be

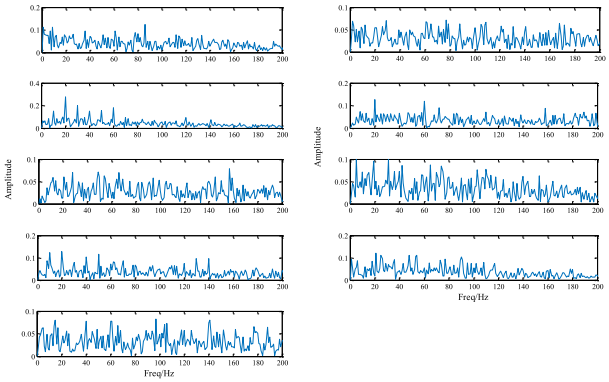

FIGURE 9. The full results of MFMD.

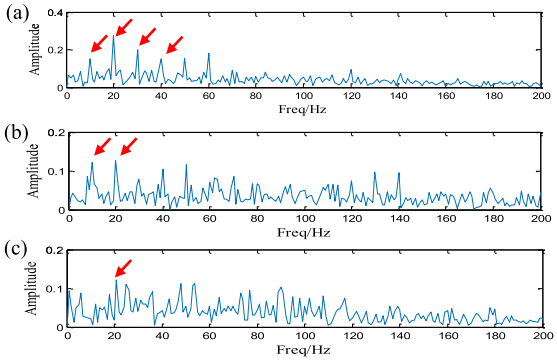

FIGURE 10. (a) The envelop spectrum of mode 3, (b) the envelop spectrum of mode 7, (c) the envelop spectrum of mode 8.

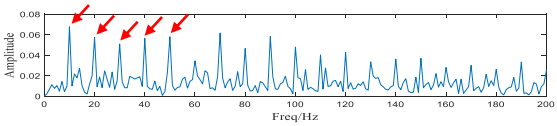

FIGURE 11. The envelop spectrum of the empirical mode.

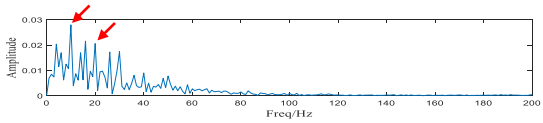

FIGURE 12. The envelop spectrum of the mode extracted by FMD.

10 and the order of the filter bank is set to be 30. The analysis result is displayed in Fig. 12, and only the modulation frequency and the second harmonic can be reluctantly found in the envelop spectrum. Therefore, FMD cannot buck the influence of strong noise hardly, because of its unreasonable parameters.

Traditional VMD is also applied, and it decomposes the simulation signal into 10 modes, which are displayed in Fig. 13. Considering that the modulation frequencies in the simulation are 800 Hz and 1800 Hz respectively, we choose mode 4 and 7 for demodulation analysis. The envelope spectra of mode 4 and 7 are shown in Fig. 14. Despite our selection, the characteristic frequency and its multiples are not clear, which means VMD is also unable to identify the characteristic frequency.

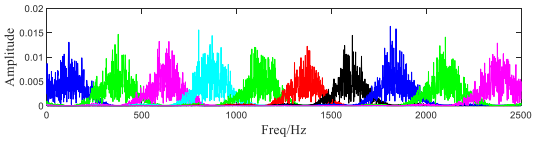

FIGURE 13. The result of VMD.

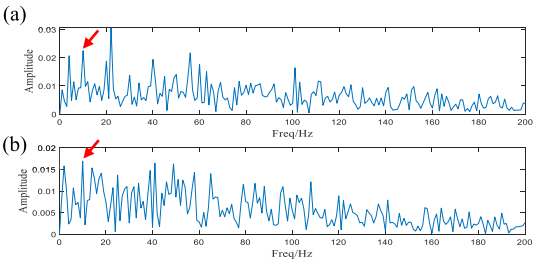

FIGURE 14. (a) The envelop spectrum of mode 4, (b) the envelop spectrum of mode 7.

V. EXPERIMENTAL VERIFICATION AND CASE ANALYSIS

A. WEAK FAULT IDENTIFICATION OF A MACHINERY FAULT SIMULATOR

A typical motor-drive-brake-type machinery fault simulator, which consists of a motor, a load and a shafting with a coupling, is built to test the influence of different mechanical faults of the ship-borne antenna drivetrain. A single-row cylindrical roller bearing with an artificial slight outer race scratch is manufactured and installed into the test rig. The test rig with the faulty bearing is displayed in Fig. 15, and the characteristic frequency of the outer race fault can be obtained as (15):

$$f_{roller} = \frac{1}{2} f_r \left[1 - \left(\frac{d}{D} \right) \cos \alpha \right] n \tag{15}$$

where f_r is the rotation frequency, n is the number of rolling elements, d is the diameter of the rolling element, D is the pitch diameter, and α is the contact angle. In the fault simulation experiment, the rotating speed is 503 rpm and the sampling frequency is set to be 12.8 kHz. Hence, the characteristic frequency of the outer race fault is calculated to be 60.85 Hz.

The original signal with its frequency spectrum and envelop spectrum are shown in Fig. 16. Due to complexity of the test rig and inevitable heavy noise, the fault features are hardly identified in the envelop spectrum. The proposed MFMD method is applied to analyze the raw signal. After scale expression, the number of the local maxima is set to be 12. Therefore, a total of 12 modes are extracted based on MFMD, and the time waveforms of all modes are illustrated in Fig. 17. Then, similar modes are merged according to their correlation coefficient. Among all merged modes, the representative one which satisfies the merged mode selection condition proposed in section III is chosen for demodulation analysis. The characteristic frequency of the outer race fault can be clearly noticed, as the envelop spectrum shows in Fig. 18.

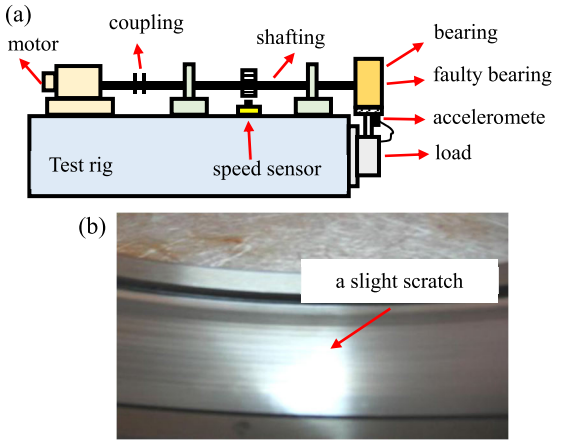

FIGURE 15. (a) The machinery fault simulator, (b) the faulty cylindrical roller bearing.

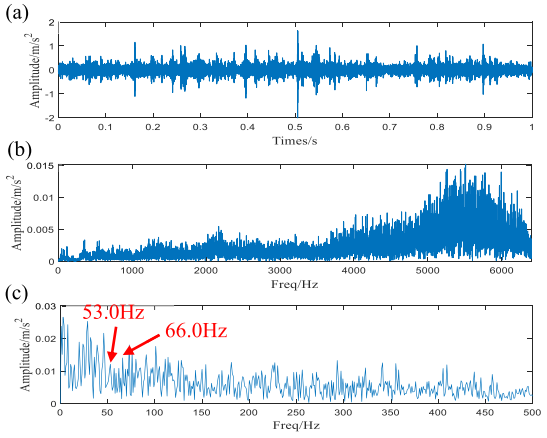

FIGURE 16. (a) The raw signal, (b) the spectrum of the raw signal, (c) the envelope spectrum of the raw signal.

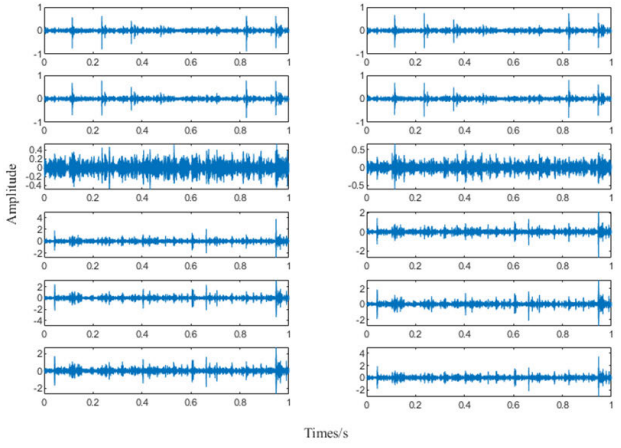

FIGURE 17. The time waveforms of all decomposed modes.

We also use EEMD [23] and Spectral Kurtosis [40] (SK) to analyze the same signal for comparison. The signal is decomposed into 14 modes by EEMD, and subsequently the envelope spectra of the first six modes are displayed in Fig. 19, for IMF 7-13 are low-frequency narrow-band signals

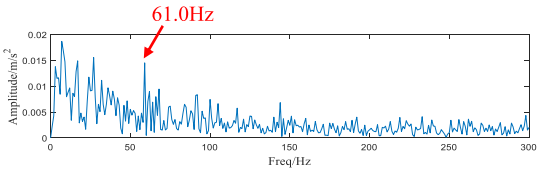

FIGURE 18. The envelope spectrum of the selected empirical mode.

without modulated fault feature. Unfortunately, there are no clear outer-race fault features found in Fig. 19, because weak fault features are totally submerged by heavy noise in the time domain. Results gained from a 3-layer Spectral Kurtosis method is displayed in Fig. 20. The sub-signal with the highest Kurtosis is located between 4800 Hz and 5600 Hz, and no fault characteristic frequency is clearly identified in its envelop spectrum as well. Therefore, a definite conclusion can be drawn that MFMD owns superior performance compared with the traditional methods.

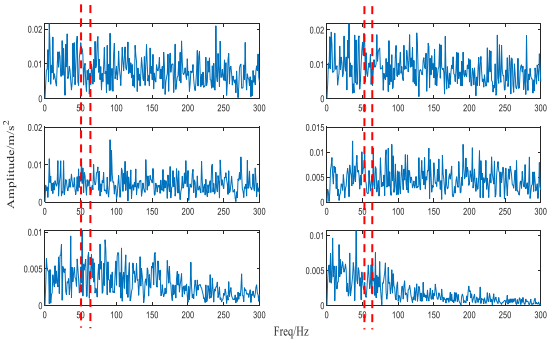

FIGURE 19. The envelope spectrum of the first six modes.

B. FAULT DETECTION FOR THE TRANSMISSION SYSTEM OF A REAL SHIP-BORNE ANTENNA

In this case, we proved that the proposed MFMD method is effective for early fault identification of the ship-borne antenna through a bearing holder fault. Generally, a transmission system of the ship-borne antennae, as shown in Fig. 21, consists of an azimuth-drive chain, a pitch-drive chain and a cross-drive chain. During a routine check before a new mission of the research ship, the engineer heard a squealing noise from the planetary reducer of the ship-borne antenna and subsequently the antenna malfunctioned. Therefore, he disassembled the planetary reducer and found that rolling elements appeared in the reducer, which means a severe bearing holder fracture. Fig. 22 shows the faulty reducer, and we can notice that the shafting slopes because the faulty bearing cannot support the weight the shafting.

However, the ship-borne antenna seemed to work properly and no abnormal phenomena, such as noise and violent vibration, were found during the previous mission. A routine spectrum analysis on board also proves that no significant fault-relative phenomena appear. The sampling rate of the health management system is 2048 Hz and signals are acquired under 1350 rpm rotating speed. Given the reduction ratio of

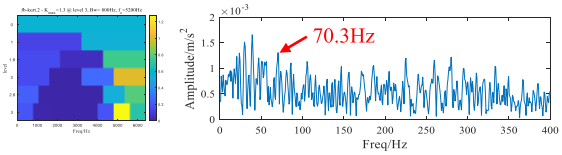

FIGURE 20. The result of SK and the envelop spectrum of the chosen sub-signal.

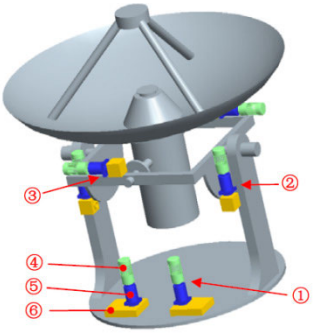

FIGURE 21. The Schematic diagram of the transmission system of a large ship-borne antenna: 1. azimuth drive chain; 2. pitch drive chain; 3. cross drive chain; 4. motor; 5. reducer; 6. gearbox.

FIGURE 22. The fault caused by the bearing holder fracture.

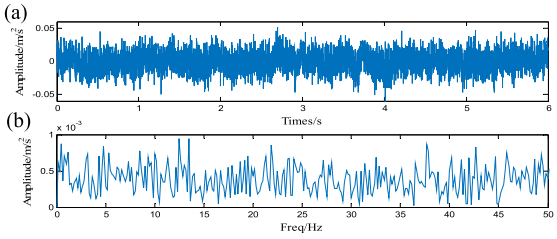

FIGURE 23. (a) The time waveform of the selected condition monitoring signal; (b) the envelop spectrum of the signal.

the planetary reducer, the fault characteristic frequency of the bearing holder is calculated to be 9.0 Hz. One of the condition monitoring signals is displayed in Fig. 23(a), with its envelope spectrum in Fig. 23(b). We can scarcely find any characteristic frequencies in the envelop spectrum, which means that the holder fault is still in the beginning stage.

Since the health management system has failed to detect the early bearing holder fault, advanced signal processing methods should be integrated into the system. As a performance test before being integrated, the proposed method is applied to extract weak fault features from condition monitoring signals. The number of the filters is set to be 9 and the order of the filter bank is 45 according to the scale expression of the frequency spectrum of the raw signal. After decomposition and combination, the most significant empirical mode is selected for demodulation analysis, as Fig. 24 shows.

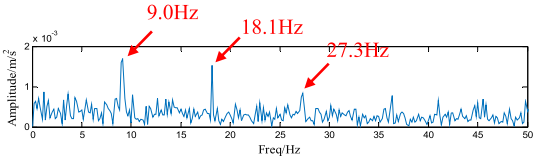

FIGURE 24. The envelop spectrum of the selected empirical mode.

Amazingly, the characteristic frequency of the holder fault 9.0 Hz with its harmonics, is found in the envelop spectrum of the selected empirical mode. Hence we can draw a conclusion that the holder of the bearing had been abraded gradually until it could not restrain the rolling elements. More importantly, the captain of the research ship allow that the proposed method is an effective feature extraction method with great potential and should be integrated on board.

We also compare the proposed MFMD method with other representative methods, especially EEMD and parameter-optimized VMD [41]. EEMD decomposes the raw signal into 14 modes, and we also selected the first 6 modes for demodulation analysis. The envelop spectra of these modes are displayed in Fig. 25, and no clear characteristic spectral lines can be found. Since the early holder fault is so weak that the periodic oscillation caused by the fault seldom appears in the time domain, EEMD cannot separate a mode which exactly contains all time-domain features of the fault, eliminating other interference and background noise.

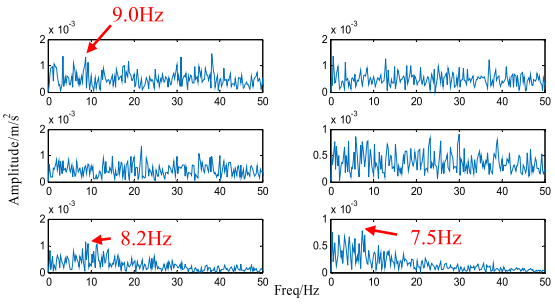

FIGURE 25. The envelop spectra of the first six modes.

Subsequently, the parameter-optimized VMD in Ref. [41] is applied for comparison. According to Ref. [41], when the optimal number of modes is 6 and the optimal bandwidth is 600, the envelope signal Kurtosis value takes the maximum of 18.17. Therefore, the raw signal is decomposed by VMD with the optimal mode number 6 and bandwidth 600, the decomposition result is shown in Fig. 26. Then we select mode 3 for demodulation analysis, because the Kurtosis value of mode 3 is the largest among all 6 modes. Fig. 3 shows the

envelop spectrum of mode 3, and in Fig. 27, we notice that the fault characteristic frequency 9.0 Hz and its harmonics disappear.

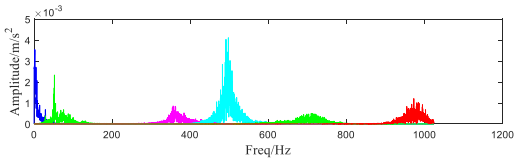

FIGURE 26. The location of each mode in frequency domain.

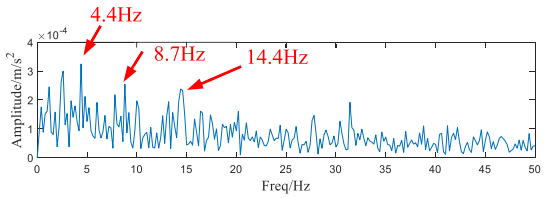

FIGURE 27. The envelop spectrum of mode 3.

VI. CONCLUSION

This paper has presented a novel fault diagnosis method for mechanical drivetrain of ship-borne antennae based on the decomposition of vibration signals using the modified FMD with adaptive parameter selection and mode combination. In the proposed method, scale-domain spectrum segmentation is employed to determine the number of filters and the order of filter bank adaptively, eliminating the effect of heavy noise caused by ship engines and obtain more meaningful modes. Since FMD tends to excessively decompose the raw signal for fault feature extraction, similar modes should be merged to enhance the expression of the weak fault feature. To this end, an effective merging method based on Pearson's correlation coefficient was proposed to form empirical modes, and we also provide an empirical mode selection norm based on CK to select the most representative one among all empirical modes.

MFMD has been applied to process a simulated signal as well as vibration signals acquired from two real cases, and comparisons between the proposed method and traditional signal decomposition methods have proved a superior performance of the proposed method. Therefore, MFMD has been integrated into the health management system on board. In general, the proposed method provides the following outstanding advantages:

1. As a concise and non-recursive method, there is no need to consider the complicated solution of the constrained variational problem and the influence of cumulative error in FMD.

2. The scale-domain expression and spectrum segmentation are applied for accurate parameter determination of FMD, reducing the influence of noise.

3. A mode merging algorithm is developed to eliminate meaningless modes and enhance fault features, ensuring effective fault identification.

4. The proposed method is self-organized so that the staff on board can easily detect mechanical faults of antennae in early stage.

However, the performances of the proposed method and original FMD highly depend on CK, which is probably influenced by other periodic interference in the mode during the iteration. In the future, a new feature-driven criterion for MFMD should be built. We also intend to develop a novel signal pre-denoising method, benefiting successive scale-domain expression and parameter optimization.

ACKNOWLEDGMENT

The authors would like to thank the staff on board and their laboratory assistants for their great support with the experiment.

REFERENCES

[1] S. He, Y. Zi, J. Chen, C. Zhao, B. Chen, J. Yuan, and Z. He, "Incipient-signature identification of mechanical anomalies in a ship-borne satellite antenna system using an ensemble multiwavelet," *Meas. Sci. Technol.*, vol. 25, no. 10, Oct. 2014, Art. no. 105006.

[2] A. L. Dias, A. C. Turcato, G. S. Sestito, D. Brandao, and R. Nicoletti, "A cloud-based condition monitoring system for fault detection in rotating machines using PROFINET process data," *Comput. Ind.*, vol. 126, Apr. 2021, Art. no. 103394.

[3] G. Manhertz and A. Bereczky, "STFT spectrogram based hybrid evaluation method for rotating machine transient vibration analysis," *Mech. Syst. Signal Process.*, vol. 154, Jun. 2021, Art. no. 107583.

[4] S. Lu, Q. He, and J. Wang, "A review of stochastic resonance in rotating machine fault detection," *Mech. Syst. Signal Process.*, vol. 116, pp. 230–260, Feb. 2019.

[5] T. Wang, Q. Han, F. Chu, and Z. Feng, "Vibration based condition monitoring and fault diagnosis of wind turbine planetary gearbox: A review," *Mech. Syst. Signal Process.*, vol. 126, pp. 662–685, Jul. 2019.

[6] Y. Li, X. Liang, Y. Chen, Z. Chen, and J. Lin, "Wheelset bearing fault detection using morphological signal and image analysis," *Struct. Control Health Monitor.*, vol. 27, no. 11, p. e2619, Nov. 2020.

[7] S. Schmidt, P. S. Heyns, and K. C. Gryllias, "A pre-processing methodology to enhance novel information for rotating machine diagnostics," *Mech. Syst. Signal Process.*, vol. 124, pp. 541–561, Jun. 2019.

[8] S. Schmidt and K. C. Gryllias, "The anomalous and smoothed anomalous envelope spectra for rotating machine fault diagnosis," *Mech. Syst. Signal Process.*, vol. 158, Sep. 2021, Art. no. 107770.

[9] B. Fang, J. Hu, C. Yang, Y. Cao, and M. Jia, "A blind deconvolution algorithm based on backward automatic differentiation and its application to rolling bearing fault diagnosis," *Meas. Sci. Technol.*, vol. 33, no. 2, Feb. 2022, Art. no. 025009.

[10] A. Kumar, C. P. Gandhi, G. Vashishtha, P. Kundu, H. Tang, A. Glowacz, R. K. Shukla, and J. Xiang, "VMD based trigonometric entropy measure: A simple and effective tool for dynamic degradation monitoring of rolling element bearing," *Meas. Sci. Technol.*, vol. 33, no. 1, Jan. 2022, Art. no. 014005.

[11] X. Yu, Z. Li, Q. He, Y. Yang, M. Du, and Z. Peng, "Gearbox fault diagnosis based on bearing dynamic force identification," *J. Sound Vib.*, vol. 511, Oct. 2021, Art. no. 116360.

[12] Y. Lei, J. Lin, Z. He, and M. J. Zuo, "A review on empirical mode decomposition in fault diagnosis of rotating machinery," *Mech. Syst. Signal Process.*, vol. 35, nos. 1–2, pp. 108–126, Feb. 2013.

[13] N. E. Huang, Z. Shen, S. R. Long, M. C. Wu, H. H. Shih, Q. Zheng, N. C. Yen, C. C. Tung, and H. H. Liu, "The empirical mode decomposition and the Hilbert spectrum for nonlinear and non-stationary time series analysis," *Proc. Roy. Soc. London A, Math., Phys. Eng. Sci.*, vol. 454, no. 1971, pp. 903–995, Mar. 1998.

[14] V. K. Rai and A. R. Mohanty, "Bearing fault diagnosis using FFT of intrinsic mode functions in Hilbert–Huang transform," *Mech. Syst. Signal Process.*, vol. 21, no. 6, pp. 2607–2615, Aug. 2007.

[15] X. Jiao, B. Jing, Y. Huang, J. Li, and G. Xu, "Research on fault diagnosis of airborne fuel pump based on EMD and probabilistic neural networks," *Microelectron. Rel.*, vol. 75, pp. 296–308, Aug. 2017.
[16] A. Mejia-Barron, M. Valtierra-Rodriguez, D. Granados-Lieberman, J. C. Olivares-Galvan, and R. Escarela-Perez, "The application of EMD-based methods for diagnosis of winding faults in a transformer using transient and steady state currents," *Measurement*, vol. 117, pp. 371–379, Mar. 2018.
[17] J. Wang, G. Du, Z. Zhu, C. Shen, and Q. He, "Fault diagnosis of rotating machines based on the EMD manifold," *Mech. Syst. Signal Process.*, vol. 135, Jan. 2020, Art. no. 106443.
[18] Y. Sun, S. Li, and X. Wang, "Bearing fault diagnosis based on EMD and improved Chebyshev distance in SDP image," *Measurement*, vol. 176, May 2021, Art. no. 109100.
[19] Y. Li, M. Xu, X. Liang, and W. Huang, "Application of bandwidth EMD and adaptive multiscale morphology analysis for incipient fault diagnosis of rolling bearings," *IEEE Trans. Ind. Electron.*, vol. 64, no. 8, pp. 6506–6517, Aug. 2017.
[20] H. Jiang, C. Li, and H. Li, "An improved EEMD with multiwavelet packet for rotating machinery multi-fault diagnosis," *Mech. Syst. Signal Process.*, vol. 36, no. 2, pp. 225–239, 2013.
[21] M. S. Hoseinzadeh, S. E. Khadem, and M. S. Sadooghi, "Quantitative diagnosis for bearing faults by improving ensemble empirical mode decomposition," *ISA Trans.*, vol. 83, pp. 261–275, Dec. 2018.
[22] H. Li, T. Liu, X. Wu, and Q. Chen, "Application of EEMD and improved frequency band entropy in bearing fault feature extraction," *ISA Trans.*, vol. 88, pp. 170–185, May 2019.
[23] H. Li, T. Liu, X. Wu, and S. Li, "Research on test bench bearing fault diagnosis of improved EEMD based on improved adaptive resonance technology," *Measurement*, vol. 185, Nov. 2021, Art. no. 109986.
[24] J. S. Smith, "The local mean decomposition and its application to EEG perception data," *J. Roy. Soc. Interface*, vol. 2, no. 5, pp. 443–454, 2005.
[25] Z. Haiyang, W. Jindong, J. Lee, and L. Ying, "A compound interpolation envelope local mean decomposition and its application for fault diagnosis of reciprocating compressors," *Mech. Syst. Signal Process.*, vol. 110, pp. 273–295, Sep. 2018.
[26] S. Sharma, S. K. Tiwari, and S. Singh, "The rotary machine fault detection by hybrid method based on local mean decomposition and fluctuation based dispersion entropy," *Mater. Today, Proc.*, vol. 43, pp. 700–705, Jan. 2021.
[27] J. Pan, J. Chen, Y. Zi, Y. Li, and Z. He, "Mono-component feature extraction for mechanical fault diagnosis using modified empirical wavelet transform via data-driven adaptive Fourier spectrum segment," *Mech. Syst. Signal Process.*, vol. 72, pp. 160–183, May 2016.
[28] S. N. Chegini, A. Bagheri, and F. Najafi, "Application of a new EWT-based denoising technique in bearing fault diagnosis," *Measurement*, vol. 144, pp. 275–297, Oct. 2019.
[29] K. Dragomiretskiy and D. Zosso, "Variational mode decomposition," *IEEE Trans. Signal Process.*, vol. 62, no. 3, pp. 531–544, Feb. 2014.
[30] Y. Wang, F. Liu, Z. Jiang, S. He, and Q. Mo, "Complex variational mode decomposition for signal processing applications," *Mech. Syst. Signal Process.*, vol. 86, pp. 75–85, Mar. 2017.
[31] Z. Li, J. Chen, Y. Zi, and J. Pan, "Independence-oriented VMD to identify fault feature for wheel set bearing fault diagnosis of high speed locomotive," *Mech. Syst. Signal Process.*, vol. 85, pp. 512–529, Feb. 2017.
[32] S. Zhu, H. Xia, B. Peng, E. Zio, Z. Wang, and Y. Jiang, "Feature extraction for early fault detection in rotating machinery of nuclear power plants based on adaptive VMD and teager energy operator," *Ann. Nucl. Energy*, vol. 160, Sep. 2021, Art. no. 108392.
[33] X. Yan, M. Jia, and L. Xiang, "Compound fault diagnosis of rotating machinery based on OVMD and a 1.5-dimension envelope spectrum," *Meas. Sci. Technol.*, vol. 27, no. 7, 2016, Art. no. 075002.
[34] X. Zhang, Q. Miao, H. Zhang, and L. Wang, "A parameter-adaptive VMD method based on grasshopper optimization algorithm to analyze vibration signals from rotating machinery," *Mech. Syst. Signal Process.*, vol. 108, pp. 58–72, Aug. 2018.
[35] M. Yonghao, Z. Ming, and L. Jing, "Identification of mechanical compound-fault based on the improved parameter-adaptive variational mode decomposition," *ISA Trans.*, vol. 84, pp. 82–95, Jan. 2019.
[36] Y. Miao, B. Zhang, C. Li, J. Lin, and D. Zhang, "Feature mode decomposition: New decomposition theory for rotating machinery fault diagnosis," *IEEE Trans. Ind. Electron.*, vol. 70, no. 2, pp. 1949–1960, Feb. 2023.
[37] X. Yan and M. Jia, "Bearing fault diagnosis via a parameter-optimized feature mode decomposition," *Measurement*, vol. 203, Nov. 2022, Art. no. 112016.
[38] Y. Miao, M. Zhao, K. Liang, and J. Lin, "Application of an improved MCKDA for fault detection of wind turbine gear based on encoder signal," *Renew. Energy*, vol. 151, pp. 192–203, May 2020.
[39] J. Gilles and K. A. Heal, "Parameterless scale-space approach to find meaningful modes in histograms—Application to image and spectrum segmentation," *Int. J. Wavelets Multiresolut. Inf. Process.*, vol. 12, no. 6, 2014, Art. no. 1450044.
[40] G. Mousmoulis, C. Yiakopoulos, G. Aggidis, I. Antoniadis, and I. Anagnostopoulos, "Application of spectral kurtosis on vibration signals for the detection of cavitation in centrifugal pumps," *Appl. Acoust.*, vol. 182, Nov. 2021, Art. no. 108289.
[41] H. Li, X. Wu, T. Liu, S. Li, B. Zhang, G. Zhou, and T. Huang, "Composite fault diagnosis for rolling bearing based on parameter-optimized VMD," *Measurement*, vol. 201, Sep. 2022, Art. no. 111637.

ZIPENG LI received the B.S. and Ph.D. degrees in mechanical engineering and automation from Xi'an Jiaotong University, Xi'an, China, in 2014 and 2020, respectively. He was a Visiting Scholar with the School of Mechanical Engineering, University of Toronto, from 2017 to 2019. Since 2020, he has been with the School of Marine Science and Technology, Northwest Polytechnic University, where he is currently an Assistant Professor with the Department of Acoustic and Information Engineering. His research interests include ocean acoustic modeling, signal processing, and pattern recognition.

ZITONG ZHOU was born in Xi'an, Shaanxi, China. He received the B.S. and Ph.D. degrees in mechanical engineering from Xi'an Jiaotong University, Xi'an, in 2014 and 2020, respectively. He is currently a Digital Engineer with the Shaanxi Key Laboratory of Gear Transmission, Shaanxi Fast Company Ltd., Xi'an. His research interests include the condition monitoring of mechanical equipment, mechanical signal processing, and the digital twin model of manufacturing.

XIAOYI ZHOU received the B.S. degree in underwater acoustic engineering from Northwest Polytechnic University, Shaanxi, China, in 2019, where she is currently pursuing the Ph.D. degree in underwater acoustic engineering. Her current research interests include signal processing, dynamics, and numerical calculation.